

Supporting Information for Electron tomography analysis of reaction path during formation of nanoporous NiO by solid state decomposition

A. K. Shukla^a, P. Ercius^b, A. R. S. Gautam^b, J. Cabana^c, U. Dahmen^b

^a*Environmental Energies Technologies Division, Lawrence Berkeley National Laboratory,
Berkeley, California, USA*

^b*National Center for Electron Microscopy, Lawrence Berkeley National Laboratory,
Berkeley, California, USA*

^c*Department of Chemistry, University of Illinois at Chicago, Chicago, Illinois, USA*

1 S.1. In-situ experiments

2 The decomposition of Ni(OH)₂ crystals was studied in-situ by exposing them
3 to the electron beam in both broad beam (TEM) and scanning probe (STEM)
4 modes. Figures S1a and S1b show bright field images for two different Ni(OH)₂
5 plates at the beginning of transformation. The transformation results in lateral
6 contraction, but negligible change in the thickness of the plate, as shown in
7 Figures S1c and S1d.

8 By rastering the beam in STEM mode over a small selected area of a Ni(OH)₂
9 crystal it was possible to induce the transformation in a localized segment (see
10 Figure S3). In this experiment, a crystal was transformed by scanning the
11 electron beam over a small area in the center of the plate, and changes were
12 observed in this crystal and an adjacent crystal, which was only heated indirectly
13 via contact with the first crystal and the substrate. This allowed the observation
14 of slow transformation on the second crystal, which was not exposed to electron
15 beam except for image acquisition. Figure S3a shows both crystals 1 and 2, at
16 the beginning of the experiment. Figure 3b shows the region in the center of
17 crystal 1 that was scanned. Continuous scanning of this small region caused
18 complete transformation of crystal 1 and partial transformation of crystal 2 and
19 other adjacent crystals, principally near the perimeter of the plate as shown in
20 Figure S3c. Figure S3d, which was taken after tilting crystal 1 to [1 1 1]_{NiO} zone
21 axis, shows that both crystals formed densified rims. This experiment confirms
22 that the transformation under the electron beam was mainly thermal, unlike
23 the observations made by Su et al [1] in Mg(OH)₂. Also, although crystal 1 was
24 exposed to localized electron dose and heating, the transformation of crystal 2
25 clearly shows that under uniform heating, the transformation begins at the edges
26 of the crystal. It should be noted that for image acquisition, low-dose, short
27 termed STEM scans were used for recording the images that did not induce any

28 noticeable transformation. This is also evident from the intermediate stages of
29 the experiment performed under a broad, parallel beam (TEM mode) shown in
30 Figure S2.

31 In another in-situ STEM experiment, a slightly tilted Ni(OH)_2 crystal was
32 scanned using an electron beam to study the initial stages of transformation.
33 Figure S4, indicates, from the mottled contrast on one of the sides of the hexag-
34 onal crystal that the transformation begins with pores running parallel to the
35 plate at the periphery of the crystal (Figure S4a corresponding to the schematic
36 drawing in Figure 6a, followed by densification of the rim, closing the path par-
37 allel to the plate and resulting in pores normal to the plate. Note the increased
38 porosity near the rim of the crystal in Figure S4b as also described in Figure
39 6b.

40 S.2. STEM tomography porosity calculations

41 The reconstructed volume was segmented manually with the help of some
42 interpolating and segmenting tools using the software Avizo[2]. In order to
43 estimate the percentage porosity, the exterior of the crystal was cropped (the
44 hexagonal outline) so that the porosity is not overestimated due to the voxels
45 outside the edge of the crystal.

46 S.3. STEM tomography error analysis

47 Electron tomography is a complex technique requiring numerous processing
48 steps to ensure quantitative results. Errors can be introduced due to imperfect
49 alignment of tilt-series, missing information at high tilts, and segmentation.
50 Figure S5 shows representative sections of the reconstructed volume and the
51 corresponding segmented volume in three orthogonal directions. To quantify
52 all significant errors simultaneously, the error analysis was performed using the
53 final segmented data and the original STEM projection near the 0° tilt an-
54 gle. The original STEM projections can be considered “ideal” projections and
55 used as a reference for the processed 3D reconstruction. The segmented data
56 is represented digitally by a 3D cube of data with $(0.34 \text{ nm})^3$ voxels (three-
57 dimensional pixels) of either pure NiO (digital 1) or pores (digital 0). The
58 voxels were summed normal to the NiO plate to produce a 2D projection with
59 intensity proportional to NiO thickness. Figure S6 shows the summation of the
60 segmented data compared to the original 0° STEM projection. The two images
61 clearly exhibit similar features, thus providing a good qualitative check of the
62 accuracy of the alignment, reconstruction and segmentation. For a quantitative
63 check, these data sets can be compared pixel-by-pixel to estimate the compound
64 error. First, the two images were registered with one another with respect to
65 magnification, position and rotation. Then each pixel in Figure S6a shows the
66 measured local mass thickness, which can be directly compared to the actual
67 local mass thickness seen in the HAADF intensity in the corresponding pixel of
68 the original STEM projection in Figure S6b. Due to the compound processing

69 error, each pixel intensity in Figure S6 corresponds to a range of pixel intensities
70 in Figure S6b. Figure S7a plots the average STEM intensity for each measured
71 local mass thickness. The standard deviation of each data point was then calcu-
72 lated, and the average error of 4.6% for all thicknesses is shown as a single error
73 bar in the lower right of Figure S7a. The ratio between the standard deviation
74 and the mean intensity for each thickness is also shown in Figure S7b which
75 range from 4% - 6%.

76 S.4. Videos

77 The following are the details of the movies available online.

78 S.4.1. Movie 1: STEM tomography

79 This movie shows the surface rendering of the 3D tomogram, followed by
80 orthogonal slices taken in two directions. Note that the pores in the center of
81 the plate go from top to bottom in a zig zag manner, while the pore distribu-
82 tion across the plane of the plate is isotropic in nature. It can be also noted
83 that the plate is denser in the center. The video also shows the pore network
84 of a section of the plate, followed by the skeletonized tomogram showing the
85 interconnectivity of these pores. The diameter of the sections in the skeleton
86 correspond to the size of the pore (scaled down five times). This is also shown
87 by using a color code (red = thick, blue = thin).

88 S.4.2. Movie 2: In-situ transformation using STEM

89 This video shows the STEM experiment described in S.1. The STEM probe
90 was scanned in the central region of crystal 1 and the changes in crystal 2 and
91 other neighboring crystals were observed.

92 References

- 93 [S1] Su, D.; Jiang, N.; Spence, J. C. H.; He, F.; Petuskey, W. T. *J. Appl. Phys.*
94 **2008**, *104*, 063514–1–063514–4.
- 95 [S2] Avizo, version 7. <http://www.vsg3d.com/>.

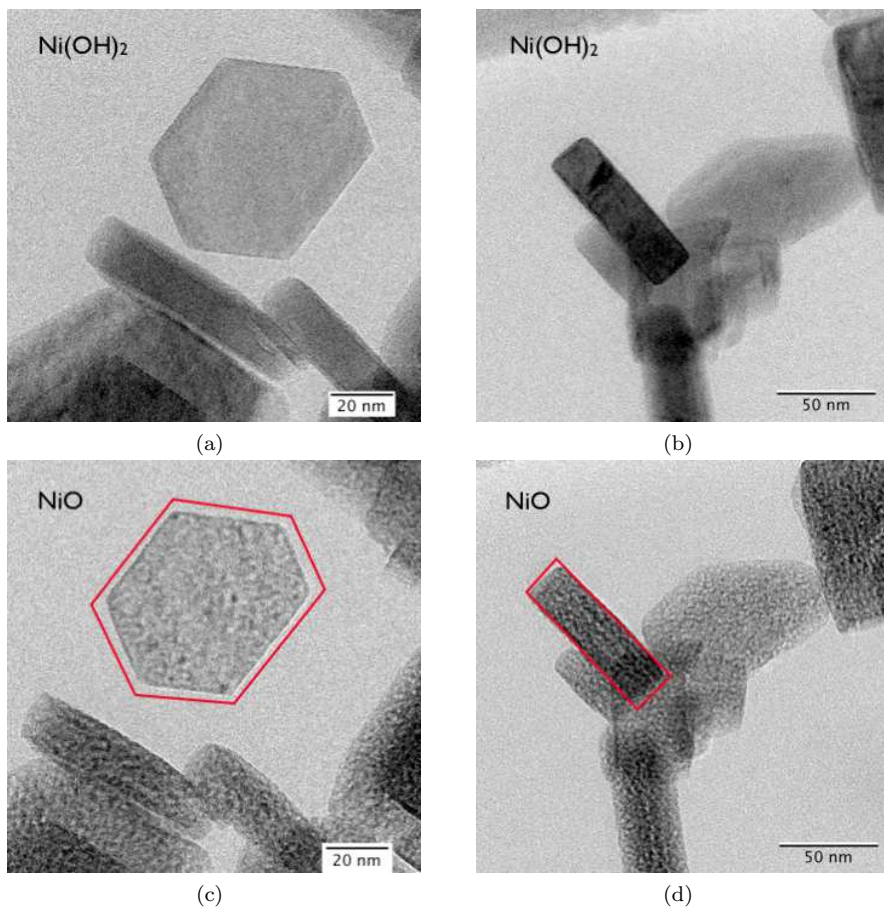


Figure S1: TEM BF images from in-situ experiment showing transformation sequence; a), b) Ni(OH)_2 crystals at the beginning of transformation; b), c) NiO crystals after transformation under the electron beam. The outline of the plate shape before the transformation shows the lateral contraction and constant plate thickness.

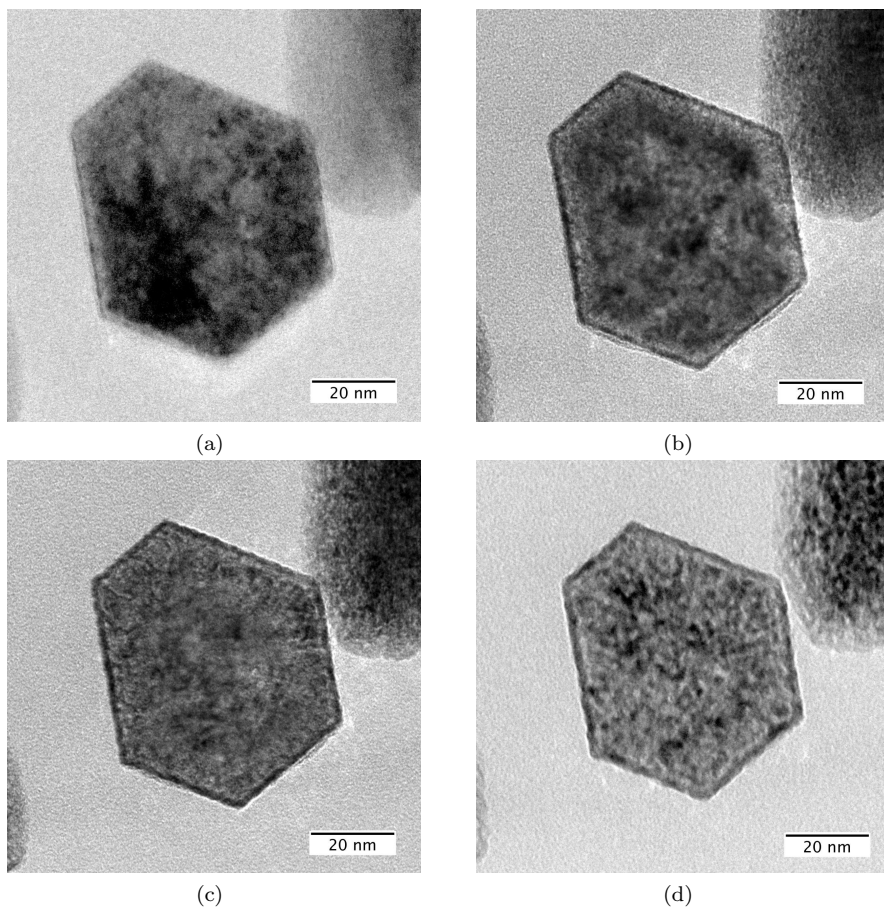


Figure S2: TEM BF images from Figure 1 in the paper reproduced with intermediate stages of transformation; a) $\text{Ni}(\text{OH})_2$ crystals at the beginning of transformation; b) and c) intermediate stages showing transformation to porous NiO on the edges of the crystal, d) NiO crystal after complete transformation under the electron beam.

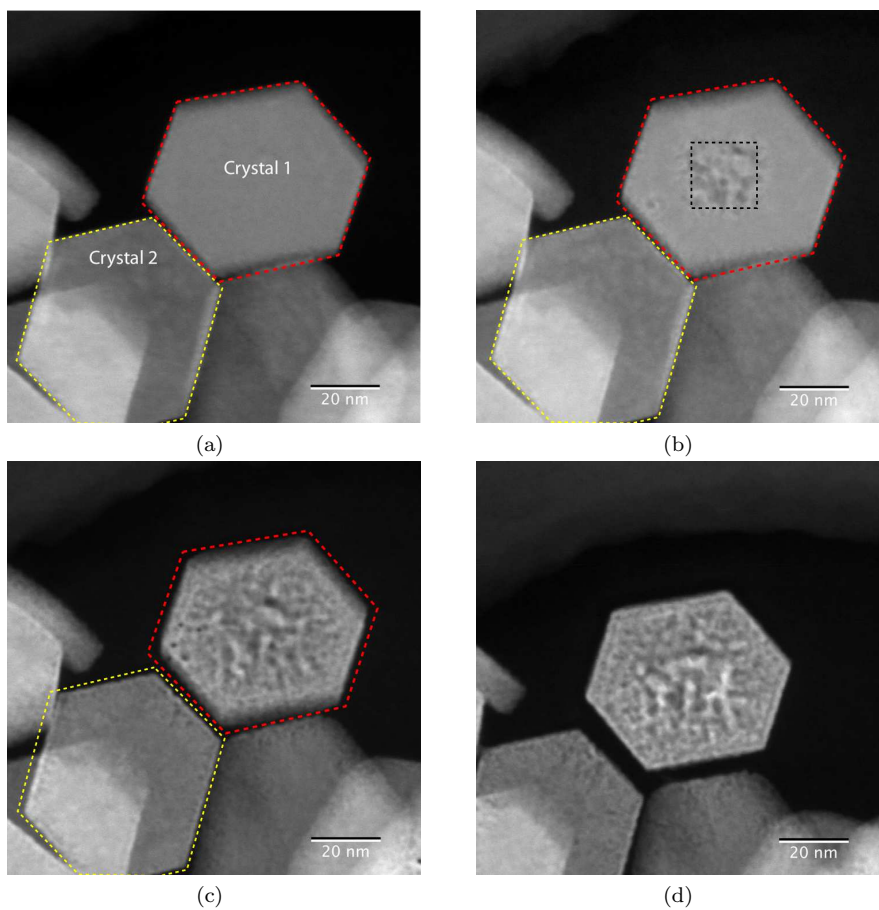


Figure S3: HAADF STEM images from in-situ experiment showing (a) Ni(OH)₂ crystals 1 and 2 at the beginning of transformation, (b) partial transformation in the center of the crystal 1 (c) partial transformation near the edges of the crystal 2 and (d) fully transformed crystal 1, tilted to zone axis. Note that during the entire experiment, only the square area shown in (b) was scanned, which indicates that the transformation was due to thermal decomposition by specimen heating.

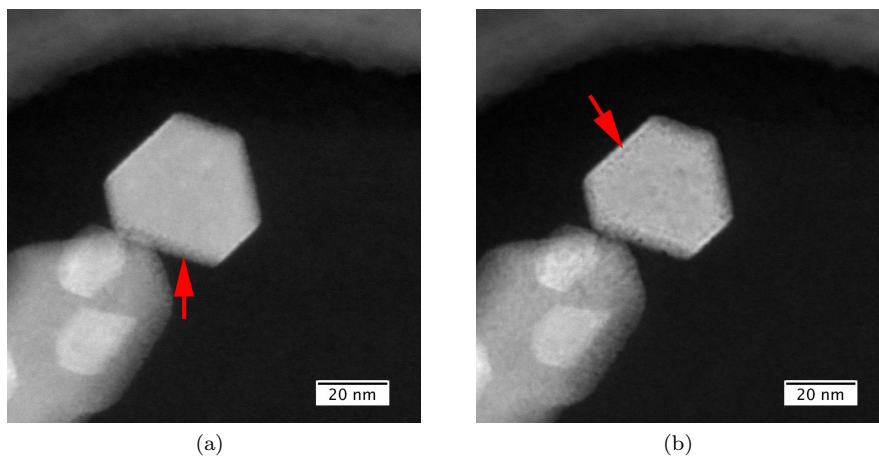


Figure S4: HAADF STEM images from in-situ experiment showing (a) mottled contrast on the side shown with a red-colored arrow indicating the early stage of transformation where the porous channels parallel to the plate are formed on the faces normal to the plate and (b) densification of the rim resulting in transport of H_2O normal to the plate as shown by the formation of porosity next to the rim indicated with a red-colored arrow.

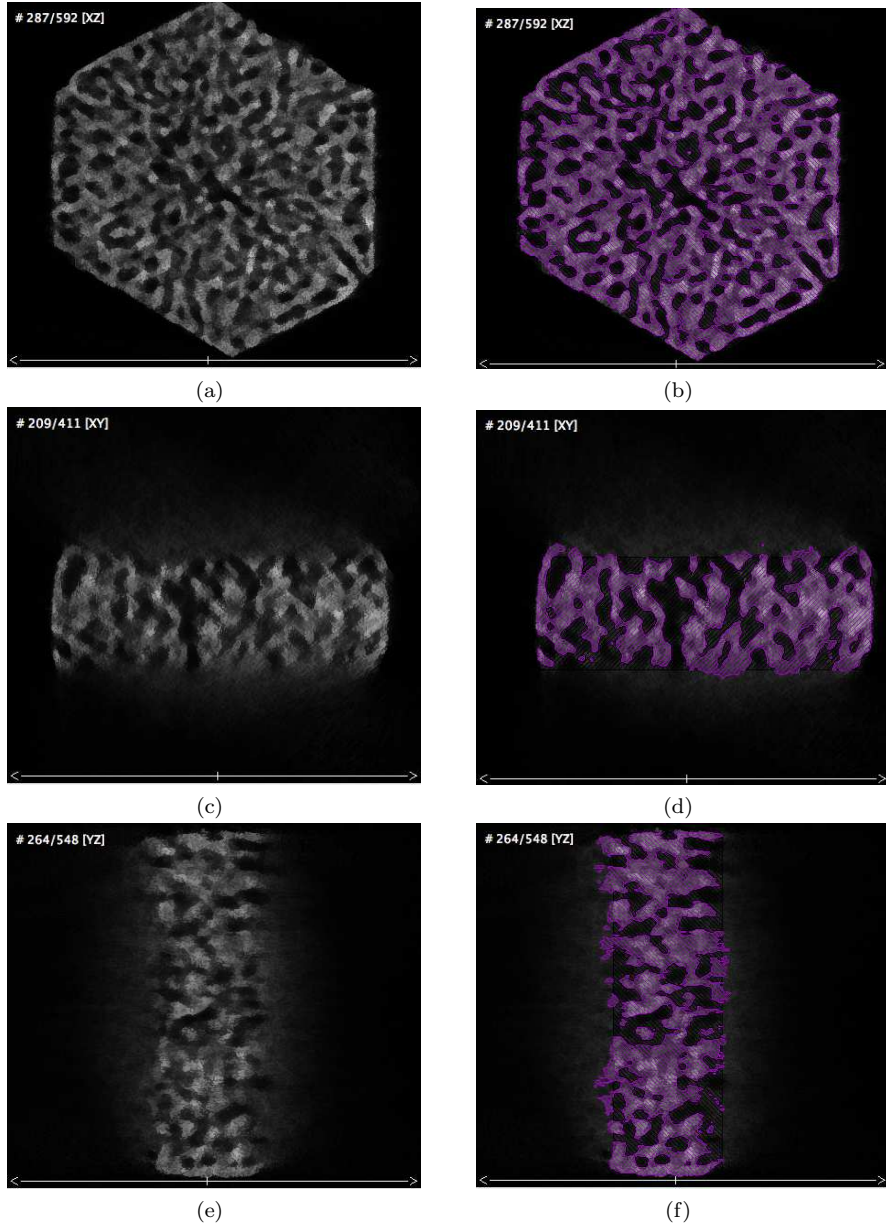


Figure S5: Slices from the reconstructed tomogram compared with those from the segmented volume.

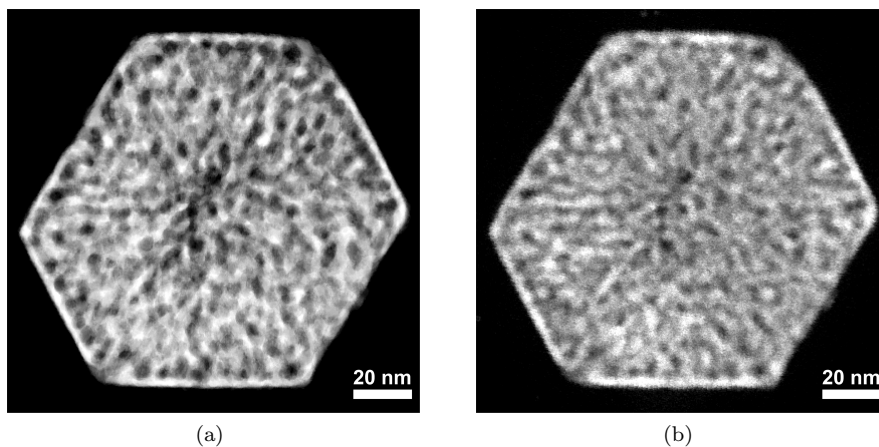


Figure S6: Images showing a) summation of the segmented data and b) original STEM image corresponding to 0° tilt.

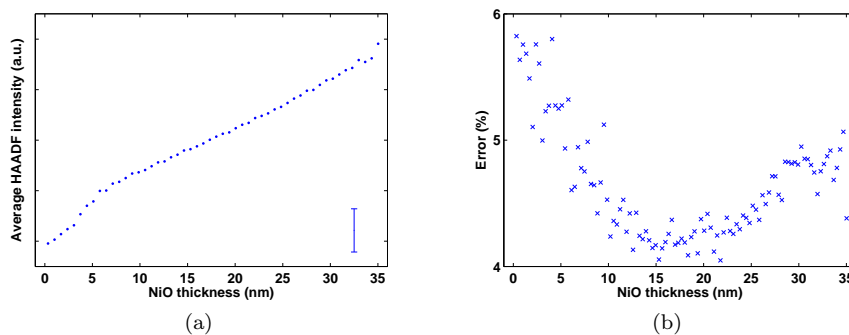


Figure S7: Error analysis showing: a) a plot of average HAADF intensity obtained from STEM image vs. equivalent thickness calculated from the segmented volume and b) distribution of error.

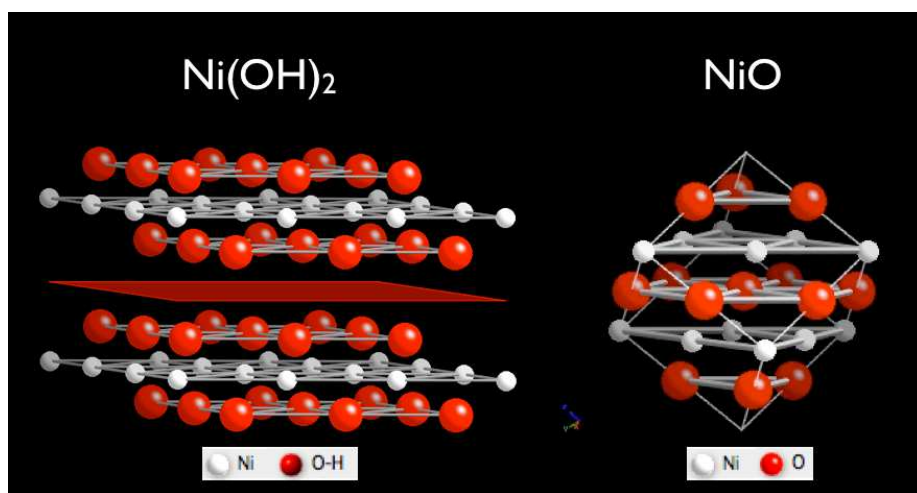


Figure S8: Comparative arrangement of close-packed planes in Ni(OH)_2 and NiO .